Journal of Solid State Chemistry **146,** 411–417 (1999)
Article ID jssc.1999.8382, available online at http://www.idealibrary.com on IDEAL®

The Electronic Structure of Hexagonal $BaCoO_3$

C. Felser,* K. Yamaura,† and R. J. Cava†

*Institut für Anorganische Chemie und Analytische Chemie, Johannes Gutenberg-Universität, Mainz, Becher Weg 24, D55099 Mainz, Germany; and †Department of Chemistry and Princeton Materials Institute, Bowen Hall, 70 Prospect Avenue, Princeton, New Jersey 08540

Received December 30, 1998; in revised form May 4, 1999; accepted May 21, 1999

TB–LMTO–ASA band structure calculations within the local spin density approximation have been performed to explain the magnetic and transport properties of $BaCoO_3$. The calculations predict a magnetic and metallic ground state as energetically favored. $BaCoO_3$ shows no long-range magnetic ordering, however, and only poor conductivity. The magnetic energy is low and the compound shows glassy susceptibility behavior at low temperatures. From the band structure we find Mott–Hubbard localization to be unlikely, and instead propose Anderson localization as a possible origin of the observed behavior. Calculations on slightly distorted structures exclude the possibility of a Peierls distortion. © 1999 Academic Press

1. INTRODUCTION

Hexagonal $BaCoO_3$ has a highly one-dimensional crystal structure formed by parallel chains of face-sharing CoO_6 octahedra separated by alkaline earth metals (Fig. 1). The face-shared octahedra allow for the possibility of metal–metal bonding due to short metal–metal contacts (1). The Co–Co distance in hexagonal $BaCoO_3$ between the two face-shared octahedra is rather short (2.38 Å), shorter than that in the metal (2.50 Å). The interchain distance is much longer (5.65 Å). These structural characteristics suggest that one-dimensional (1-D) electronic states may occur. $BaCoO_3$ is a semiconductor with transport by *n*-type carriers. The origin of the semiconducting behavior is not clear. Under the assumption of low-spin Co^{4+} (t_{2g}^5, e_g^0) a gap within the t_{2g} states can be produced in different ways: (i) Strongly correlated electrons may produce an energy gap at the Fermi level through a Mott–Hubbard-type transition, or (ii) a Peierls distortion due to a dimerization of Co within the Co chains along the *c* axis might be possible. (iii) The semiconducting behavior arises not as a result of an energy gap but because of a mobility gap: 1-D localization due to undetected disorder in the structure, resulting in charge carriers being scattered by random centers. This is particularly effective in low-dimensional systems and would lead to an Anderson localization.

The temperature dependence of the electrical resistivity suggests activated conductance or 1-D localization (2). The intrachain spin interactions are found to be ferromagnetic, but long-range magnetic ordering has not yet been observed. This may in part be due to the triangular arrangement of the ferromagnetic chains, for which partially frustrated long-range order among the chains is expected if the interactions between chains are antiferromagnetic. These open questions have motivated us to perform spin-polarized band structure calculations on $BaCoO_3$.

2. CRYSTAL STRUCTURE AND COMPUTATION DETAILS

$BaCoO_3$ crystallizes in the hexagonal perovskite structure ($P6_3/mmc$ (No. 194), $a = 5.645$ Å, $c = 4.752$ Å) (Fig. 1). The structure type is generally known as the $2H$ type: the stacking sequence unit along the *c* axis has two CoO_6 layers before repeating and the symmetry is hexagonal. We use the experimentally determined lattice constants and atomic positions for the calculation. The self-consistent band structure calculation has been performed within the local density approximation (LDA) to investigate the nonmagnetic ground state and within the local spin density approximation (LSDA) for the spin-polarized ground state (3) using the LMTO–ASA method. A detailed description of the LMTO–ASA method has been given elsewhere (4–7). The calculations were semirelativistic; i.e., all relativistic effects were taken into account except for ther spin–orbit coupling. The angular momentum expansion of the basis functions included $l = 3$ for barium and $l = 2$ for Co and O. The O *s* and the Ba *f* states were treated by a special down-folding procedure. The *k*-integrated functions were evaluated by the tetrahedron method (8) on a grid of 969 *k* points in the irreducible part of the Brillouin zone (BZ). The BZ is as described in Ref. (9), with the symmetry points and lines labeled in accordance with the standard notation. The band structure was calculated for the Bloch vectors along the following lines: Γ (0, 0, 0) to K ($\frac{2}{3}$, $\frac{1}{3}$, 0) to M ($\frac{1}{2}$, 0, 0) to Γ and

0022-4596/99 $30.00

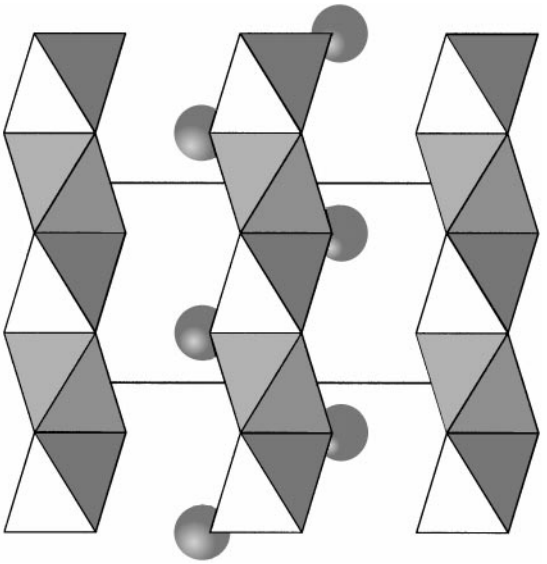

FIG. 1. Crystal structure of $BaCoO_3$ projected down [110]. The face-shared CoO_6 octahedra form chains running along [001]. The spheres are the Ba atoms.

TABLE 1
Peierls Distortion of $BaCoO_3$ with Different Co–Co Distances (Space Group of the Distorted Structure: $P\bar{6}m2$ (No. 187)

Short Co–Co distance in Å	ΔE_{tot} (eV)	μ_B	Metal	With oxygen relaxation
2.38	0	1	Yes	No
2.31	3.2	1	Yes	No
2.31	1.9	1	Yes	Yes
2.26	3.2	1	Yes	No
2.16	3.1	0	No	No

Note. The sum of the two Co distances are always 2×2.38 Å. The inclusion of oxygen relaxation means that oxygen triangles are situated in between two Co.

from A $(0, 0, \frac{1}{2})$ to L $(\frac{1}{2}, 0, \frac{1}{2})$ to H $(\frac{2}{3}, \frac{1}{3}, \frac{1}{2})$ to A in units of $(2\pi/a, 2\pi/a, 2\pi/c)$.

To study the bonding situation in the vicinity of the Fermi level, two relatively new tools of the LMTO program package have been used. The orbital character of each band can easily be visualized with the aid of the so-called fat band representation (10), where each band is plotted with a width weighted by the eigenvector contribution of the relevant orbital: 100% orbital contribution corresponds to 0.05, the size of the energy axis or 0.25 eV. The second tool is the so-called COHP (crystal orbital Hamilton population) (11), the density of states weighted by the corresponding Hamiltonian matrix elements. The calculation of the "Peierls distorted" structures with alternating short and long Co–Co contacts along the c axis were performed using the experimental lattice constants but reduced symmetry (see Table 1), within the nonisomorphic subgroup $P\bar{6}m2$ (No. 187), because the Co positions are no longer related by a screw axis.

3. ELECTRONIC STRUCTURE

3.1. Density of States

An overview of the electronic properties derived from the calculations is shown in Fig. 2. Panel (a) shows the total density of states of paramagnetic $BaCoO_3$, panel (b) shows the spin-polarized total DOS, panel (c) shows the majority (spin-up) and minority (spin-down) states of Co d, and panel (d) shows the partial DOS of oxygen p, again separated into the two spin directions. Due to the crystal field of Co surrounded by oxygen in an octahedral arrangement, we also expect in these hexagonal perovskites a splitting of t_{2g} (d_{xy}, d_{xz}, d_{yz}) and e_g $(d_{z^2}, d_{x^2-y^2})$ bands, within the internal coordinate system, as is found in the cubic perovskites.

The high charge on Co^{4+} would result in short Co–O distances and hence a strong crystal field. As a result, we would expect low-spin Co^{4+} in $BaCoO_3$. For this low-spin $BaCoO_3$ we expect a metallic ground state from simple

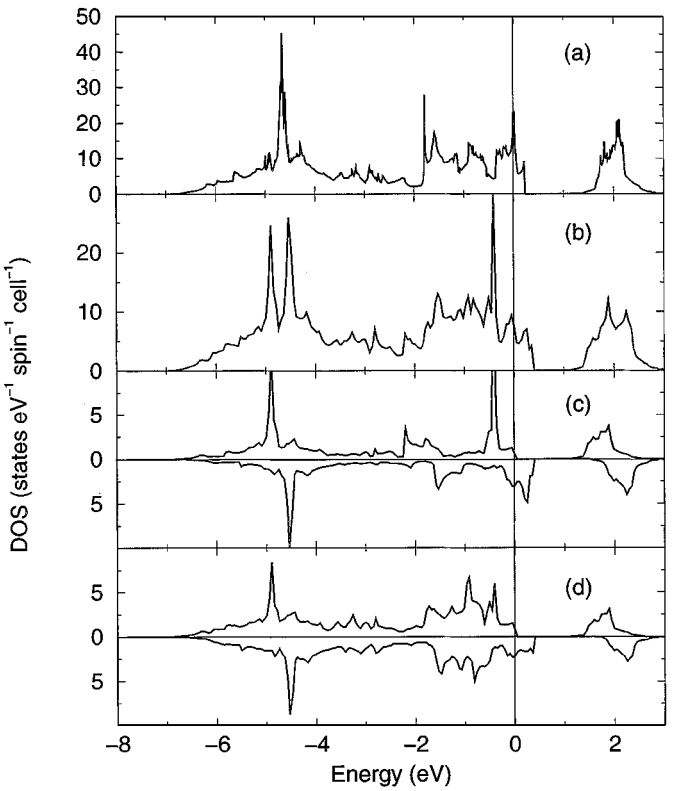

FIG. 2. Total LMTO–ASA density of states for $BaCoO_3$. (a) Total paramagnetic density of states (DOS), (b) total spin-polarized DOS, (c) partial DOS of Co upper panel majority band and lower panel minority band, and (d) partial spin-polarized DOS of oxygen $2p$ electrons, both spin directions. The vertical lines mark the Fermi energy.

electron counting due to the presence of two holes in the t_{2g} band (t_{2g}^5, e_g^0). In the paramagnetic DOS shown in panel 2(a), a high density of states is found at the Fermi level (11 states eV^{-1} $spin^{-1}$). Such a peaked DOS is an indication that a magnetic ground state would be preferred. To avoid high density of states, the system choses to spin polarize. In panel (b) it is seen that, for the magnetic calculation within the LSDA, the density of states at E_F is substantially reduced (3.2 states eV^{-1} $spin^{-1}$) for a ferromagnetic arrangement of Co within the chains. The Fermi energy is situated in a pseudogap between two peaks. From the energetics viewpoint the magnetic ground states is therefore preferred. The calculated magnetic energy is 0.08 eV per unit cell, and therefore the magnetic and nonmagnetic ground states are nearly degenerate. The calculated magnetic energy is of the same order of magnitude as the experimentally determined magnetic coupling ($J = 10$ K). From this we can conclude that the Hubbard U is not important in this system because the one-electron value (which ignores electron correlations) is very near to that observed experimentally.

The calculated magnetic moment per primitive unit cell is 2 μ_B, i.e., 1 μ_B per Co atom, but the polarization of the Co 3*d* electrons is small within the sphere of one Co (-0.69). The magnetic moment on Co also polarizes the density of states of oxygen (0.09 per O). Ba is unaffected; it is mainly an electron donor. The calculations show that $BaCoO_3$ is clearly not a band insulator. The Co 3*d* majority and minority states are shown in panel (c). As expected for low-spin Co^{4+}, all majority Co t_{2g} states are filled and are separated by a gap of 1.3 eV from the e_g majority bands. The two holes within the t_{2g} minority band are responsible for the metallic nature of the ground state of this compound, in agreement with the temperature-dependent magnetic susceptibility, which suggests the same electron configuration (2). Again, the e_g states for the minority spins are separated by a gap from the t_{2g} states. The oxygen states in a spin-polarized representation are shown in panel (d). Due to the strong Co–O interaction, the oxygen states are also polarized. The polarization of oxygen states is observed in the region of the Co e_g states (the states which form a σ-type bonding with oxygen) as well as in the region of the t_{2g} states (π-type interaction). From the density of states we can conclude that the semiconducting behavior cannot be explained easily from the band structure.

3.2. *Spin-Polarized Band Structure and Crystal Orbital Hamiltonian Populations*

The spin-polarized band structure diagrams are presented in Fig. 3, in the left panels. Fig. 3(a) shows the spin-polarized band structure of the $BaCoO_3$ majority (spin-up) bands and Fig. 3(b) the minority bands. Γ to K to M to Γ are the directions perpendicular to the c axis (the axis of the one-dimensional chains of CoO_6 octahedra) within the

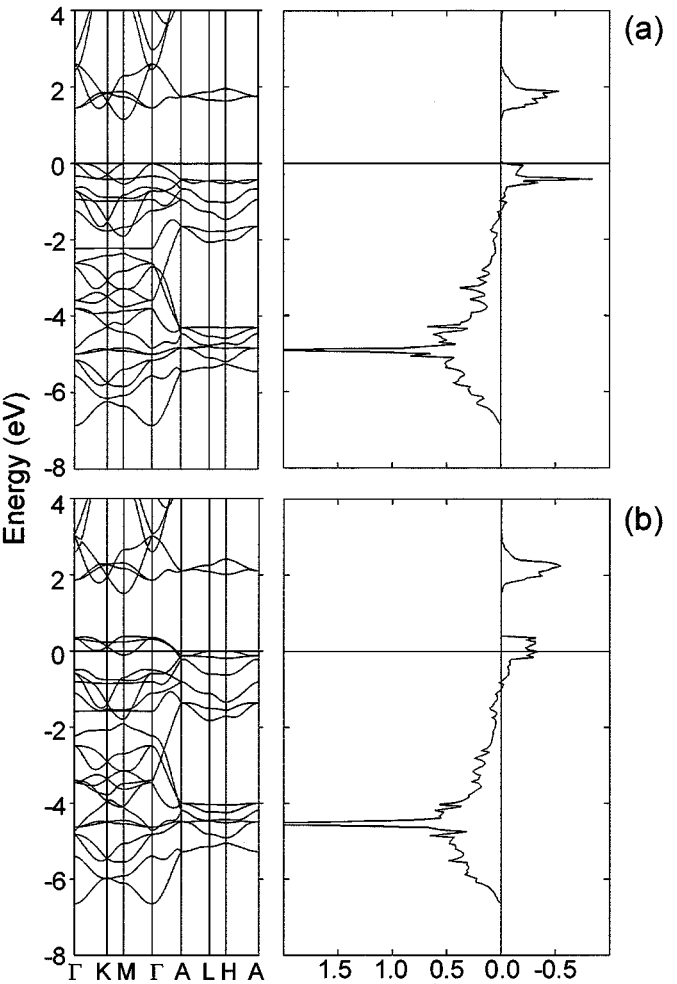

FIG. 3. LMTO–ASA band structure for (a) the majority band structure of $BaCoO_3$, together with the COHP of the Co–O interaction for this spin direction. (b) The minority band structure together with Co–O interaction (spin-down).

Brillouin zone. From Γ to A, along c^* in the reciprocal space, the direction of the chains in real space, the dispersion of the bands are the highest due to the strong metal–metal interactions within the chains. At the edge of the Brillouin zone all bands are doubly degenerate, due to the presence of a translational symmetry element, the screw along the c axis. The points A, L, and H at the edges of the BZ therefore have translational contributions. Because there are two formula units in the primitive unit cell, we expect 18 oxygen p bands (nine degenerate bands at the edge of the BZ) and 10/5 d bands of cobalt. As known from the DOS, all t_{2g} majority bands are filled, whereas there are two holes in the minority t_{2g} band as expected for Co^{4+}. In both spin directions, the t_{2g} bands overlap with the oxygen bands and are separated from the e_g bands by a direct gap of 1.3 eV. The disperson in all directions perpendicular to the one-dimensional chains is small. Thus, from the viewpoint of the electronic structure

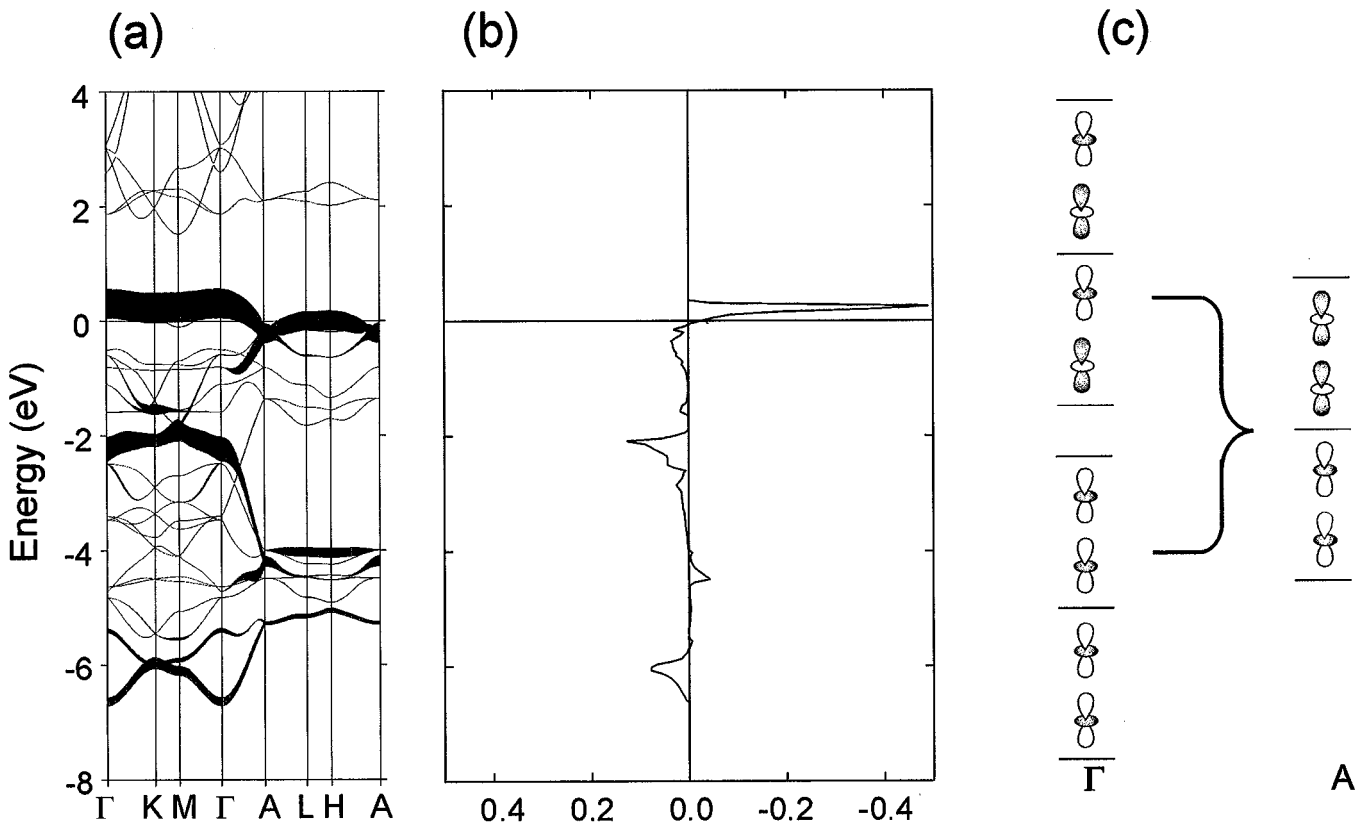

FIG. 4. (a) Fat bands of $BaCoO_3$ projected on the Co–Co σ-type interaction mediated by d_{z^2} orbitals, 100% eigenvector contribution corresponds to a 0.6-eV width. The corresponding COHP, metal–metal σ-type interaction. (c) Scheme of d_{z^2} orbitals mediating the σ-type metal–metal interaction in $BaCoO_3$. Orbital interaction at Γ and A.

this compound seems to be quasi-one-dimensional. Only the e_g bands, which are empty, have a significant dispersion also in the direction perpendicular to the chains. The σ-type Co–O interaction therefore has some band character. This one dimensionality of the electronic structure leads to the possibility that the system could be unstable with respect to structural distortions.

To analyze the bonding situation in detail, and to picture the orbitals, the COHPs of the different bonding interactions in $BaCoO_3$ have been investigated. In the right panels of Figs. 3(a) and 3(b) the COHPs of the Co–O interaction are shown for both spin directions, in the same energy range as that in the band structure. The strong metal–nonmetal interaction is the cause for the polarization of the oxygen states. The Co–O interaction is bonding in the range of the oxygen states and becomes antibonding in the range of the metal states. The interaction can be separated into a σ-type interaction mediated by Co e_g orbitals and a π-type interaction mediated by t_{2g} orbitals, respectively. Whereas the π^* bands are found below E_F in Fig. 3(a) (majority bands), they are situated in the vicinity of the Fermi level in Fig. 3(b) (minority bands). Separated from these bands by a band gap, the σ^* bands are found above E_F in both cases. Apart from the metal–metal interaction, the metal–oxygen interactions also contribute to the states at E_F.

To clarify questions regarding which interaction is responsible for the difference in the observed and calculated transport properties, we investigate the bonding situation within the one-dimensional metal chains. The fat-band projections of the Co–Co σ-type interaction are mediated by the d_{z^2} orbitals in Fig. 4(a), together with the COHP of this special bonding in Fig. 4(b). Because the strength of the bonding interactions is unaffected by the spin polarization (the minority bands are shifted only by an energy of 0.5 eV relative to the majority band, the exchange energy), we can consider only one spin direction. Although the Co–O interaction is important, the metal–metal interaction dominates in this structure type. Whereas the crystal field splitting of the Co d orbitals into t_{2g} and e_g bands is defined within the internal coordinate system of the octahedra orientated along [110], we discuss the bonding interaction between the Co atoms by building a chain along the c axis within the crystallographic coordinate system. A σ-type interaction between Co would be mediated by the d_{z^2} orbital, whereas the d_{xz} and d_{yz} orbitals build a π-type interaction. As seen in the fat-band representation of the Co d_{z^2} orbitals, we

observe two fat bands (at -2 and 0.5 eV), due to the two Co atoms per unit cell, along the direction Γ to K to M to Γ within the BZ. Because of the additional Co–O interaction, which is not totally separated from the metal–metal interaction, we also find contributions of these eigenvectors to some oxygen bands. At the edges of the BZ (A to L to H) these two bands are degenerate because the two Co atoms in the unit cell are related to each other by a translation of (0, 0, 0.5). This fact can be easily understood with the aid of our orbital scheme (Fig. 4(c)). If the d_{z^2} orbitals of the two Co atoms in the unit cell are in phase at the Γ point, the interaction is bonding and these orbitals contribute mainly to the lower fat band 2 eV below E_F. In the case that the two orbitals are not in phase, an antibonding interaction results in an orbital contribution to the fat band 0.5 eV above E_F along Γ to K to M. Due to the chain of equally spaced Co atoms in the c direction, the bonding and the antibonding band are degenerate at the A point, although there are two Co atoms per unit cell. At all points in the BZ with a c^* contribution, the orbitals of the neighboring unit cell provide a phase shift in the z direction and therefore the bonding as well as the antibonding bands are degenerate. This leads to one d_{z^2} band fat band along A to L to H. This is important for the electronic properties of the compound. Only a break of the symmetry (Peierls distortion) could render a gap at E_F possible.

3.3. An Investigation of Possible Peierls Distortions

To answer the question of whether a Peierls distortion makes sense for $BaCoO_3$, we have performed so-called frozen phonon calculations, allowing for changes in the Co–Co distances, i.e., Co–Co dimerization, without a relaxation of the oxygen. Due to the reduction of symmetry (e.g., no traslational symmetry element in the c direction), the space group is now $P\bar{6}m2$ (No. 187). The corresponding band structures are displayed in Figs. 5a–c and 5e. This permits us to investigate how large the alternation of distances would have to be to obtain a gap at E_F. Figures 5b and 5d differ in that in the latter case we have also changed the positions of the oxygen (see Table 1) without affecting the symmetry. For example, for Fig. 5c the atomic positions are given in Table 2.

The driving force for any geometrical distortion of the Peierls type would come from those occupied energy levels that lie at the highest energy. In our case, this is the metal–metal $dd\sigma^*$ interaction together with the metal–nonmetal $dp\pi^*$ interaction. Both interactions contribute to the minority bands crossing E_F. From the geometrical view point, the energy minimum would correspond to the undistorted structure. Thus, the energetics of a Peierls distortion need to overcome the inherent stiffness of the underlying structural framework to convert the metal into a semiconductor. The comparison of the total energies found in the frozen phonon calculations shows that even in the case of a small distortion the energy change is large and predicts the undistorted structure as the preferred one. We also investigated the effect of allowing the oxygen positions to relax. This results in some changes, but the undistorted structure remains favored. The small changes in the structure, however, change the band structure slightly. Figure 5a shows the band structure of undistorted $BaCoO_3$. A change of the

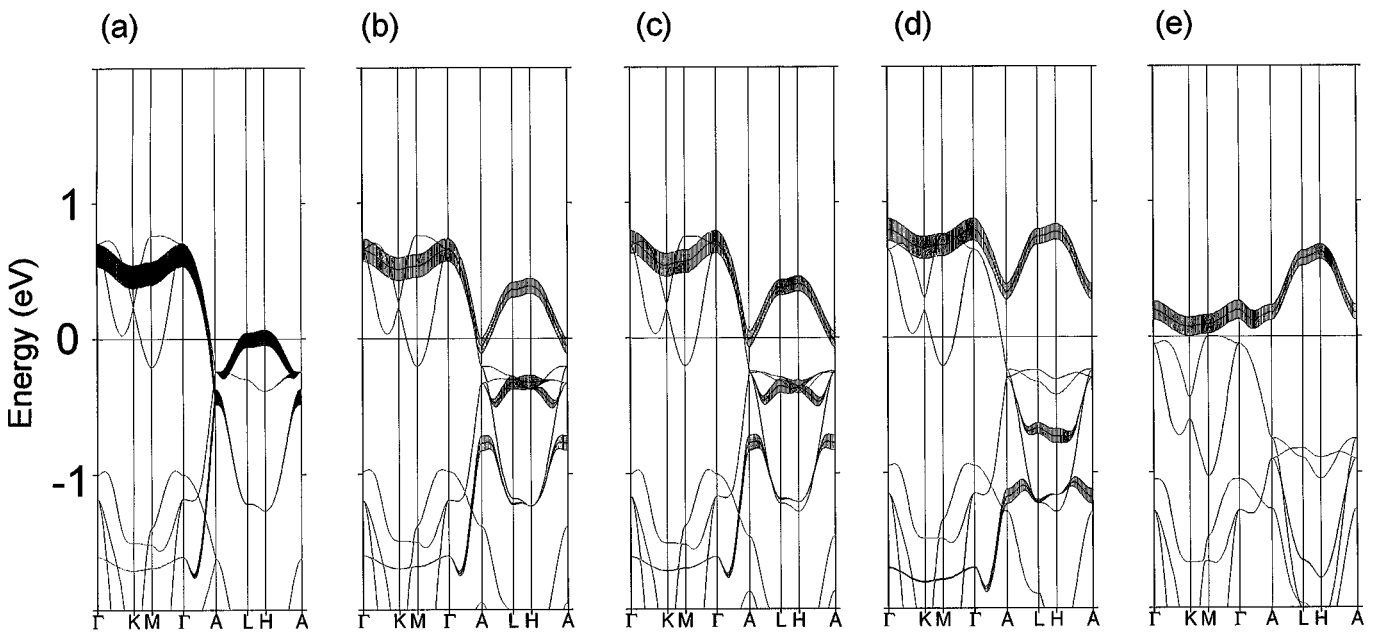

FIG. 5. LMTO band structure calculation for the "Peierls" distorted structure of $BaCoO_3$ for different Co–Co distances (see Table 1) within the space group of the distorted structure: $P\bar{6}m2$ (No. 187).

TABLE 2
Atomic Positions for the Distorted Structure (*c*)

Atom	Position x	y	z
Ba1	$-\frac{1}{3}$	$\frac{1}{3}$	0.0
Ba2	$\frac{1}{3}$	$-\frac{1}{3}$	0.5
Co	0.0	0.0	0.25594
O1	−0.2964	−0.1482	0.0
O2	0.2964	0.1482	0.5

symmetry due to allowing for two different Co atoms (one Co–Co distance of 2.31 Å, the second of 2.45 Å) in Fig. 5b changes the behavior of the metal d_{z^2} fat band strongly, but leaves the Co–O bands uneffected. At the *A* point, the upper fat band the antibonding metal band dips below the Fermi energy, building a small hole pocket, whereas the bands due to the Co–O interaction (not drawn as fat bands) cross E_F. With a change of the oxygen position such that the triangles of oxygen are always situated between two cobalt atoms, one obtains a "pseudogap" in the metal–metal band, whereas the band due to the contribution of the Co–O interaction still crosses E_F (Fig. 5c). Even differences of the Co–Co distance of nearly 0.25 Å lead to a magnetic and metallic ground state (Fig. 5d). A strong distortion (one Co–Co distance of 2.6 Å and the other of 2.16 Å) that yields the band structure shown in Fig. 5e makes a gap in the band structure possible and leads to a nonmagnetic ground state. The Co–O bands are situated below E_F, whereas two metal bands, one for each spin direction, are found above E_F, separated by a gap of less than 0.1 eV. Such a large structural change would be clearly seen in an X-ray pattern, even in powder diffraction. A Peierls distortion for a chain of face-shared octahedra seems to be unlikely because of the strong bonding interaction between two neighboring octahedra. Apart from the strong metal–metal bonding, the two octahedra share three oxygen atoms, making the structure very stiff.

4. DISCUSSION

The overall band structure is quasi-one-dimensional as is expected for a structurally one-dimensional system and in agreement with the experimental observations. From the viewpoint of the calculation, the magnetic ground state correponding to ferromagnetic arrangement of the spins within the Co chains is energetically favored. Then the high-temperature behavior of the susceptibility curve can be understood under the assumption of a ferromagnetic (spin $-\frac{1}{2}$) intrachain spin interaction. This is in agreement with the theoretically found low-spin configuration for Co^{4+} (t_g^5, e_g^0). The interaction between the chains could be ferromagnetic or antiferromagnetic, but the former is ruled out because bulk ferromagnetism is not seen. An antiferromagnetic long-range ordering between the chains is, from the viewpoint of symmetry, not eaily formulated. Since the chains are arranged in triangles, there is no simple scheme for obtaining a suitable supercell that would permit bulk antiferromagnetic coupling to propagate through the solid—the system is frustrated as are the delafossites $CuYO_{2+\delta}$ (12). The anomalies seen in the low-temperature experiments could be the signature of antiferromagnetic interactions associated with the "glassy" behavior of the chain–chain interaction.

The question about the origin of the semiconducting behavior of this compound can also be addressed with the results of our calculations. The calculation results in a metallic ground state. The possibility to be considered was that a Mott–Hubbard transition, due to strongly correlated electrons, takes place. For two low-spin Co^{4+} crystallizing in the space group $P6_3/mmc$, a Mott–Hubbard transition is not possible due to the symmetry of the hexagonal space group. Apart from the point symmetry, this space group is determined by an additional translation symmetry element. This symmetry element connects both Co atoms within the unit cell by a translation of (0, 0, 0.5). Therefore, the bands of the two Co atoms are degenerate at the edge of the BZ. Within the local spin density approximation, each spin direction is calculated nearly independantly. Therefore, one band of the spin-polarized band structure is occupied by one electron. For semiconducting behavior one band of one spin direction, a minority band must be separated from the other. Such a separation is not possible through a Mott–Hubbard transition in this space group because of the degenerate character of the bands at the edge of the BZ. Only a structural distortion (Peierls distortion or disorder) can render a gap at E_F possible. The second possibility is that dimerization due to a Peierls distortion leads to the space group $P\bar{6}m2$, without the Co atoms related by a transitional symmetry element. Our frozen phonon calculations have shown that a strong structural distortion is necessary to get a gap at E_F. The cause for this is the strong bonding interaction along *c*. Apart from the strong metal–metal interaction, the face sharing of neighboring octahedra would discourage an alternation of Co–Co bond lengths. Therefore, a Peierls distortion as a cause for the semiconducting behavior also appears to be excluded. The final possibility, Anderson localization, seems to be the most reasonable explanation. Metallic behavior, in terms of the temperature dependence of the resistivity, is usually not compatible with 1-D chains because of its inherent instability—any defective link in the chain can cause localization. Further characterization of the properties would be necessary to finally resolve these issues within the context of the band structures described here.

ACKNOWLEDGMENTS

This work was supported by the Fond der chemischen Industrie. O. K. Andersen, O. Jepsen, G. Krier, and A. Burckhardt are thanked for

providing the LMTO program and for their support and encouragement. C.F. thanks R. Seshadri and W. Tremel for discussions and E. Rochholz for help with the plots.

REFERENCES

1. C. N. R. Rao and B. Raveau, "Transition Metal Oxides." Wiley–VCH, New York, 1998.
2. K. Yamaura, H. W. Zandbergen, and R. J. Cava, submitted.
3. U. von Barth and L. Hedin, *J. Phys.* **C4,** 2064 (1971).
4. O. K. Andersen and O. Jepsen, *Phys. Rev. Lett*. **53,** 2571 (1984); O. K. Andersen, Z. Pawlowska, and O. Jepsen, *Phys. Rev. B* **34,** 5253 (1986).
5. O. K. Andersen, O. Jepsen, and D. Glötzel, *in* "Highlights of Condensed-Matter Theory" (F. Bassani, F. Fumi, and M. P. Tosi, Eds.), North-Holland, New York, 1985.
6. O. K. Andersen, *Phys Rev. B* **12,** 3060 (1975).
7. H. L. Skriver, "The LMTO Method." Springer, Berlin, 1984.
8. O. Jepsen and O. K. Andersen, *Solid State Commun.* **9,** 1763 (1971).
9. C. J. Bradley and A. P. Cracknell, "The Mathematical Theory of Symmetry in Solids." Clarendon, Oxford, 1972.
10. O. Jepsen and O. K. Andersen, *Z. Phys. B* **97,** 35 (1995).
11. F. Boucher, O. Jepsen, and O. K. Andersen, unpublished results.
12. R. J. Cava, H. W. Zandbergen, A. P. Ramirez, H. Takagi, C. T. Chen, J. J. Krajewski, W. F. Peck, Jr., J. V. Waszczak, G. Meigs, R. S. Roth, and L. F. Schneemeyer, *J. Solid State Chem.* **104,** 437 (1993).